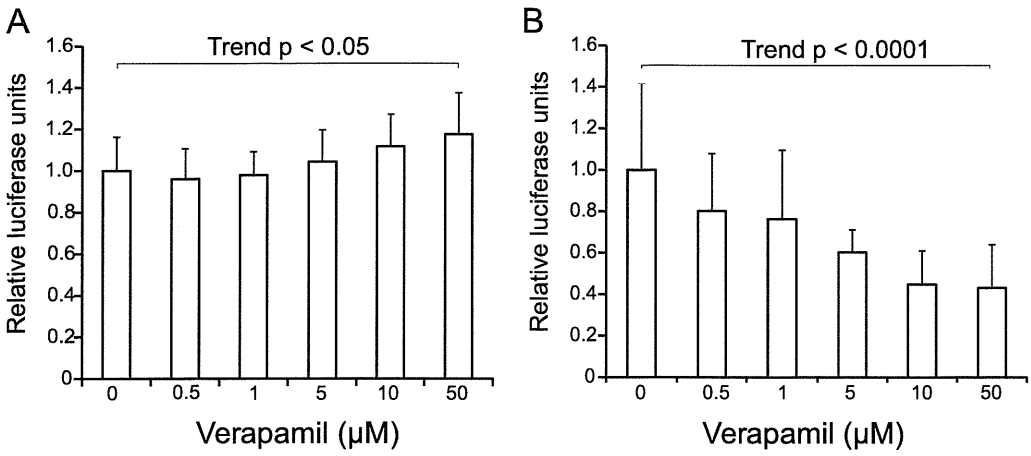

Figure 1. Verapamil activates *FRZB* promoter and reduces Wnt/β-catenin signaling. Luciferase activities in human chondrosarcoma (HCS) cells treated with the indicated concentrations of verapamil for 24 hrs. Firefly luciferase activity for *FRZB* promoter (A) or TOPFlash reporter activity (B) are normalized by the TK promoter-driven Renilla luciferase activity and expressed as relative luciferase units. The mean and SEM ($n=12$) are indicated. ** $p<0.01$ and *$p<0.05$ versus control by one-way ANOVA with Tukey's test.
doi:10.1371/journal.pone.0092699.g001

Drug repositioning strategy, in which a drug already used for a specific disease is applied to treat another disease, has been gaining increased attention from both academia and industry in recent years [18,19]. The advantage of this strategy is that the identified drugs can be readily applied to clinical practice, because the optimal doses, adverse effects, and contraindications are already established.

Here, we screened FDA-approved compounds to identify a clinically applicable drug that induces *FRZB* gene expression and downregulates Wnt/β-catenin signaling. We identified that one of calcium channel blockers, verapamil, but not other blockers upregulates expression of the *FRZB* gene and induces chondrogenic markers. In chondrogenically differentiated ATDC5 and explants of mouse tibiae, verapamil blocks nuclear localization of β-catenin and induces proteoglycan production. Finally, articular injection of verapamil ameliorated cartilage damages in OA-induced knees in rat model.

Materials and Methods

Screening of FDA-approved drugs with dual luciferase reporter assay

The *FRZB* promoter region (positions −2,218 to −1 immediately upstream of the ATG translation start site) was amplified with primers, 5′- ccgCTCGAGTGTAGACCAGGCAAAGTTTGTA-3′ and 5′- ggaAGATCTGGATCTGGGAGCTTCTCCTC-3′, from human genomic DNA isolated from HEK293 cells, in which the 5′ overhangs are indicated by lower case letters and the XhoI and BglII sites are underlined. The amplicon was cloned into pGL4.10-luc2 luciferase vector (Promega) using XhoI and BglII sites (pGL4.10-*FRZB*). Human chondrosarcoma (HCS-2/8) cells were kindly provided by Dr. Masaharu Takigawa at Okayama University [20], and were cultured in Dulbecco's Modified Eagle's Medium (DMEM, Invitrogen) supplemented with 10% fetal bovine serum (FBS, Thermo Scientific). For the *FRZB* promoter assay, $\sim 1\times10^4$ cells were seeded in 96-well culture plates (Falcon) and were transfected with the pGL4.10-*FRZB* as well as phRL-TK encoding Renilla luciferase (Promega) using Fugene6 (Invitrogen) according to the manufacturer's protocols. For measuring β-catenin-mediated transcriptional activation, HCS-2/8 cells were transfected with TOPFlash firefly luciferase reporter vector (M50 Super 8× TOPFlash plasmid, Addgene) and phRL-TK. At 24 hours after transfection, the cells were incubated for 24 additional hours in the presence of 10 μM of 1,186 FDA-approved chemical compounds (Prestwick Chemical). Luciferase activity was measured using the Dual Luciferase Reporter Assay System (Promega) and PowerScan4 (DS Parma Biomedical). Firefly luciferase activity was normalized by Renilla luciferase activity and relative luciferase units (RLU) are indicted.

Total RNA extraction and real-time RT-PCR analysis

The human studies including using HCS-2/8 cells were approved by the Ethical Review Committee of the Nagoya University Graduate School of Medicine. Human osteoarthritic chondrocyte (OAC) cells were obtained from patients who underwent joint replacement for knee OA after appropriate written informed consent was obtained. The conditioned medium enriched with mouse Wnt3A (Wnt3A-CM) was harvested from L Wnt-3A cells (CRL-2647, ATCC) that stably expressed mouse Wnt3a. OAC cells were treated with variable combinations of verapamil, recombinant human Wnt3A (R&D systems), Wnt3A-CM, and 20 mM LiCl. Total RNA was isolated from OAC cells using Trizol (Life Technologies). The first strand cDNA was synthesized with ReverTra Ace (Toyobo). We quantified mRNAs for *FRZB*, *ACAN*, *COL2A1*, *SOX9*, *AXIN2*, and *MMP3* using LightCycler 480 Real-Time PCR (Roche) and SYBR Green (Takara). The mRNA levels were normalized for that of *GAPDH*.

Knockdown of *FRZB* using siRNA

OAC cells were transfected with siFRZB-1 (5′- GGCUAAAGUUAAAGAGAUA -3′and 5′-UAUCUCUUUAACUUUAGCC-3′) or siFRZB-2 (5′- GGAUCGACUCGGUAAAAAA -3′ and 5′-UUUUUUACCGAGUCGAUCC -3′) using Lipofectamine 2000 (Life Technologies) according to the manufacturer's protocols. Four hours after transfection, the medium was changed to fresh DMEM with 10% FBS, and cells were treated with Wnt3A-CM and 25 μM of verapamil.

Western blotting

OAC cells were treated with Wnt3A-CM as well as with 0, 2.5, 5, 10, and 25 μM of verapamil. After 72 hours, cells were lysed in

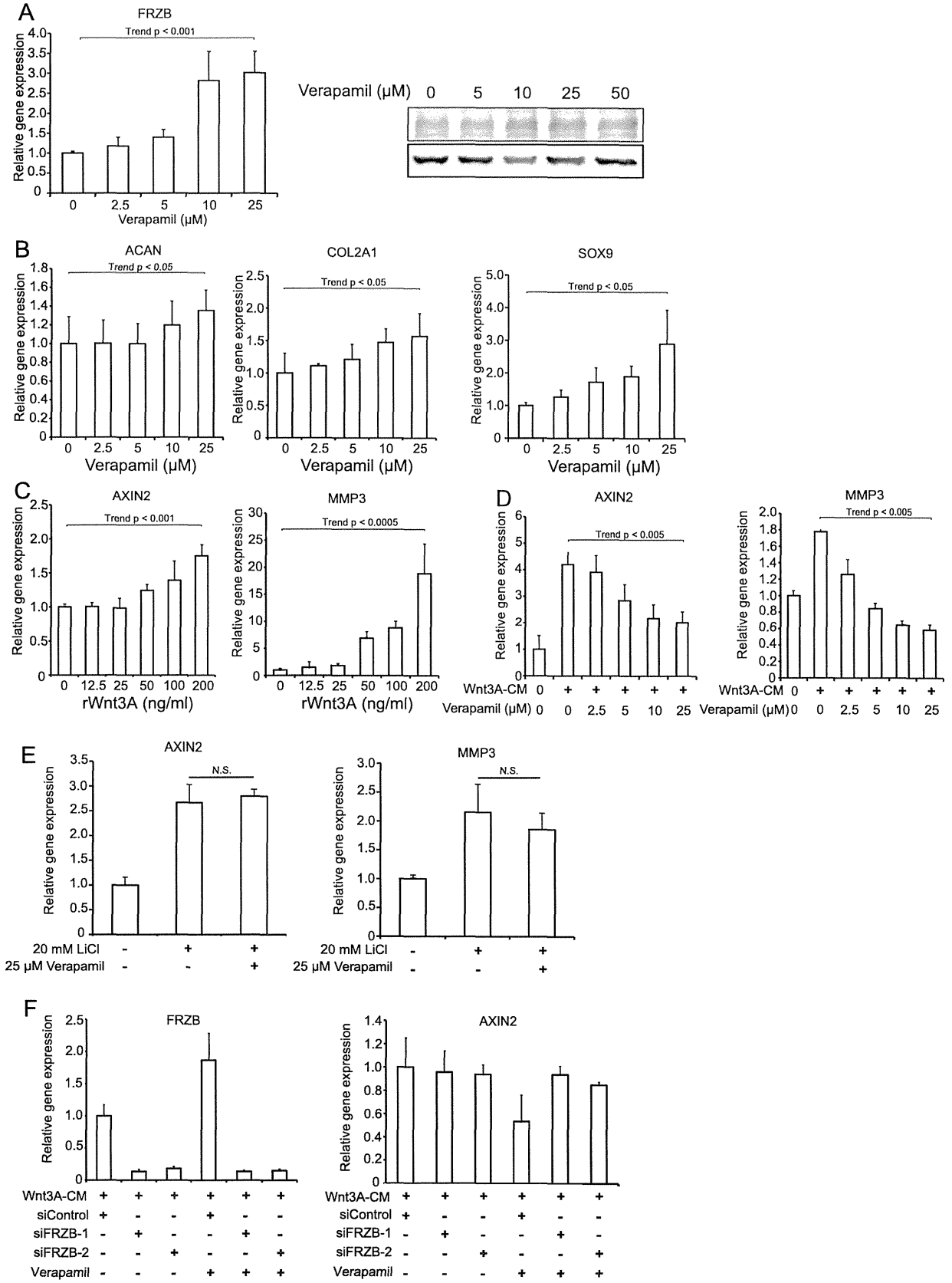
A
FRZB
Trend p < 0.001
Relative gene expression
Verapamil (μM)
Verapamil (μM) 0 5 10 25 50
B
ACAN
Trend p < 0.05
COL2A1
Trend p < 0.05
SOX9
Trend p < 0.05
C
AXIN2
Trend p < 0.001
MMP3
Trend p < 0.0005
rWnt3A (ng/ml)
D
AXIN2
Trend p < 0.005
MMP3
Trend p < 0.005
Wnt3A-CM
Verapamil (μM)
E
AXIN2
N.S.
MMP3
N.S.
20 mM LiCl
25 μM Verapamil
F
FRZB
AXIN2
Wnt3A-CM
siControl
siFRZB-1
siFRZB-2
Verapamil

Figure 2. Verapamil upregulates chondrogenic makers (*ACAN* encoding aggrecan, *COL2A1*, and *SOX9*) and downregulates Wnt-responsive *AXIN2* and *MMP3* in human osteoarthritic chondrocytes (OAC) cells. Expression levels of each mRNA are normalized to that without treatment. (A) Verapamil upregulates the native *FRZB* at the mRNA and protein levels in OAC cells ($n=3$). (B) Gene expressions of *ACAN*, *COL2A1*, and *SOX9* are increased by verapamil in 24 hrs. Purified Wnt3A protein increases *AXIN2* and *MMP3* mRNA expressions in 24 hrs (C), and verapamil inhibits the Wnt3A-induced gene expressions (D). (E) Verapamil does not suppress LiCl-induced *AXIN2* and *MMP3* expressions. (F) *FRZB* siRNAs (siFRZB-1 and siFRZB-2) cancel the effects of verapamil in Wnt3A-treated OAC cells. The mean and SEM ($n=3$) are indicated. *$p<0.05$ versus control by one-way ANOVA with Tukey's test.
doi:10.1371/journal.pone.0092699.g002

the ice-cold RIPA Lysis Buffer (Santa Cruz) supplemented with 0.1 mM dithiothreitol, 1 μg/ml leupeptin, 1 mM phenylmethylsulfonyl fluoride, and 1 μg/ml aprontinin. Whole cell lysates were separated on SDS-PAGE and transferred to a nitrocellulose membrane followed by immunoblotting with anti-β-catenin (BD Transduction Laboratories) and anti-β-actin (C4, Santa Cruz) antibodies.

Alcian blue staining

ATDC5 cells were supplied by the Riken BioResource Center (Tsukuba, Japan). ATDC5 cells were cultured in DMEM/F12 (a mixture of Dulbecco's modified Eagle's medium and Ham's F12 medium) (Sigma–Aldrich) supplemented with 5% fetal bovine serum (FBS, Thermo Scientific). ATDC5 cells were differentiated into chondrocytes with insulin-transferrin-selenite (ITS, Invitrogen) for two weeks, and were treated with Wnt3A-CM as well as with 0, 2.5, 5, 10, and 25 μM verapamil. After 72 hours, cells were fixed with methanol for 30 minutes at −20°C, and stained overnight with 0.5% Alcian Blue 8 GX (Sigma) in 1N HCl. For quantitative analyses, Alcian blue-stained cells were lysed in 200 μl of 6 M guanidine HCl for six hours at room temperature. The optical density of the extracted dye was measured at 630 nm using PowerScan 4 (DS Pharma Biomedical).

Immunofluorescence staining

OAC were fixed with 4% paraformaldehyde at room temperature. Coronal paraffin sections of proximal tibial growth plates were deparaffinized and hydrated in xylene. The specimens were then treated with a blocking buffer including 2% goat serum in 0.5% Triton-X100 for 60 minutes and incubated with mouse anti-β-catenin antibody (BD Transduction Laboratories, 1:500 dilutions for the cells and 1:100 dilutions for the sections) at 4 °C overnight. The specimens were incubated with goat anti-mouse fluorescein isothiocyanate (FITC) secondary antibody (1: 500 dilution) at room temperature for one hour. Finally, the specimens were mounted in VectaShield containing 1.5 μg/ml DAPI (Vector Laboratories, Peter-borough, UK) and visualized using IX71 (Olympus). The ratio of β-catenin-positive cells were automatically estimated by dividing FITC-positive cells by the number of DAPI-positive nuclei using MetaMorph (Molecular Device)

Explant culture of tibiae of mouse embryo

All animal studies were approved by the Animal Care and Use Committee of the Nagoya University and the animals were sacrificed under deep anesthesia, if necessary. maintained according to the guidelines for the care of laboratory animals of the Gifu International Institute of Biotechnology. Tibiae of wild type mouse embryo (E17.5) were dissected under the microscope, placed in a 24-well plate, and cultured in α-minimal essential medium (Invitrogen) supplemented with 0.2% bovine serum albumin, 1 mM β-glycerophosphate, and 50 μg/ml ascorbic acid. Embryonic tibiae were further treated with 20 mM LiCl or with 0, 25, and 50 μM verapamil for 10 days, then fixed in 10% formaldehyde in phosphate-buffered saline, demineralized with 0.5 M EDTA, and embedded in paraffin. Sections were stained with hematoxylin-eosin and Alcian blue. Hypertrophic cells were defined as having a length along the longitudinal axis greater than 10 μm under light microscopy. The numbers of hypertrophic chondrocytes were counted by two blinded observers and averaged.

In vivo generation of OA and its morphological evaluation

Wistar/ST rats were deeply anesthetized with an intraperitoneal injection of pentobarbital sodium (10 mg/ml×0.1 ml). Under sterile conditions, the right knee was induced to osteoarthritis by resection of the menisco-tibial ligament to destabilize medial meniscus (DMM surgery). Verapamil (50 μM) in 50 μl PBS was intraarticularly injected into the right knee each week. The skin and joint capsule on the left knee was incised (sham side). At four and eight weeks postoperatively, rats were sacrificed and tissue around the knees was fixed overnight in 4% paraformaldehyde at 4 °C, dehydrated, and embedded in paraffin. The sagittal sections were stained with Safranin O and Fast-green. OA progressions were graded according to the modified Mankin histologic score on both tibial and femoral sides of articular cartilages [21,22]. The modified Mankin score was a sum of the following seven parameters: articular cartilage structure, grades 0–11; tidemark duplication, grades 0–3; Safranin O staining, grades 0–8; fibro-cartilage, grades 0–2; chondrocyte clones in uncalcified cartilage, grades 0–2; hypertrophic chondrocytes in calcified cartilage, grades 0–2; and subchondral bone, grades 0–2. The grades of OA were estimated by two blinded observers and averaged.

Screening of verapamil-activated signaling pathways that facilitate upregulation of *FRZB*

For screening for involvement of other signaling molecules in verapamil-mediated activation of FRZB promoter, HCS-2/8 cells were co-transfected with the pGL4.10-*FRZB* and pCMV-SPORT6 Smurf1 (IMAGE clone 3660965, DNAFORM) or pCMV-SPORT6 Smurf2 (IMAGE clone 5345689, DNAFORM) and phRL-TK. At 24 hours after transfection, the cells were incubated for 24 additional hours in the presence of 50 μM of Verapamil with specific inhibitors of other signaling, SP600125 (JNK inhibitor), PD98059 (Erk inhibitor). Luciferase activity was measured using the Dual Luciferase Reporter Assay System (Promega)

Statistical analysis

Data are presented as the mean ± SEM. Statistical significance was determined either by unpaired t-test or one-way ANOVA followed by Tukey's post-hoc test. The Jonckheere-Terpstra trend test was used to assess dose responses, and is indicated by a letter 'trend' followed by a p value. Although one-way ANOVA gave more stringent values than the Jonckheere-Terpstra trend test,

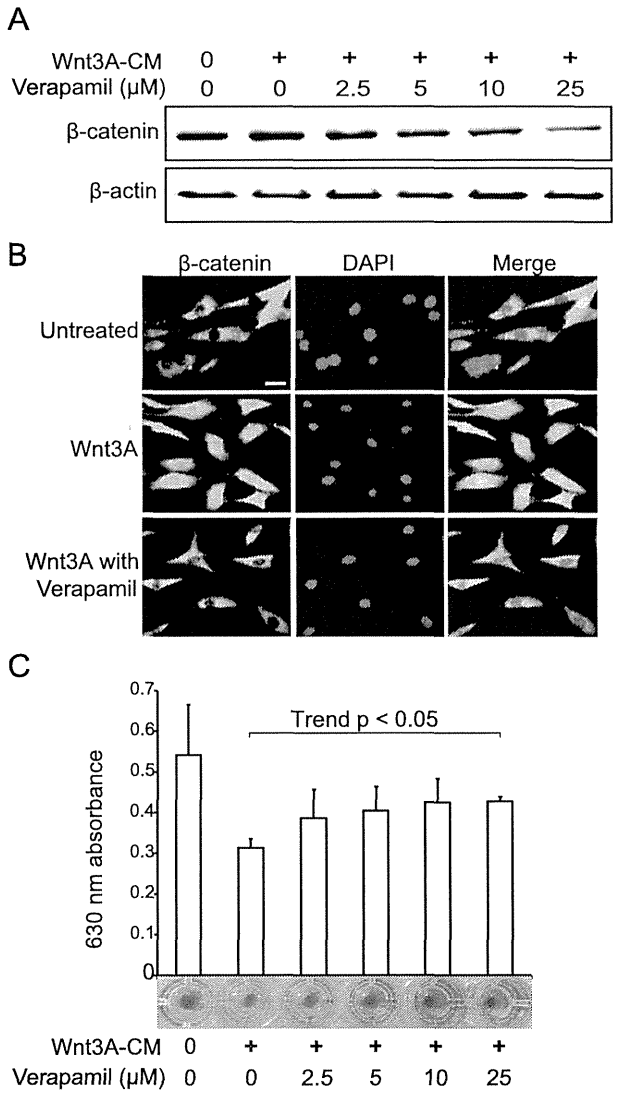

Figure 3. Verapamil suppresses Wnt-mediated protein expression and nuclear translocation of β-catenin in human osteoarthritic chondrocytes (OAC) cells, and verapamil rescues Wnt-induced loss of proteoglycans in chondrogenically differentiated ATDC5 cells. (A) Immunoblotting of β-catenin in OAC cells treated with Wnt3A-CM and verapamil for 72 hrs. (B) Immunofluorescence staining with anti-β-catenin antibody in OAC cells. Untreated cells (upper panels), cells treated with Wnt3A-CM alone (middle panels), and cells treated with Wnt3A-CM and 25 μM verapamil (lower panels) for 72 hours are stained with anti-β-catenin antibody (green, left panels) and DAPI (blue, middle panels). Wnt3A-induced nuclear localization of β-catenin is blocked by verapamil. Scale bar = 20 μm. (C) Alcian blue staining of ATDC5 cells that are differentiated to chondrocytes with ITS for two weeks. The cells are subsequently treated with Wnt3A-CM and verapamil for 72 hrs. Proteoglycans are quantified by measuring the optical density at 630 nm of the cell lysates. The mean and SEM (n = 3) are indicated. *$p<0.05$ versus control by one-way ANOVA with Tukey's test.
doi:10.1371/journal.pone.0092699.g003

one-way ANOVA was not suitable for estimating dose responses. P-values less than 0.05 were considered significant. The statistical analyses were performed with SPSS Statistics 21 (IBM).

Results

Verapamil enhances the *FRZB* promoter activity and reduces Wnt/β-catenin signaling activity

To identify a clinically applicable compound for OA, we transfected HCS-2/8 cells with either pGL4.10-*FRZB* to estimate the *FRZB* promoter activity or TOPFlash to estimate the Wnt/β-catenin activity. We searched for a compound that enhances the *FRZB* promoter and suppresses the Wnt/β-catenin activity among FDA-approved chemical compounds (Prestwick Chemical). These assays were repeated three times and we chose 41 best compounds. With the 41 compounds, we further repeated the assays three additional times. After the first and second rounds of screening, we chose 18 best compounds that consistently exhibited beneficial effects (data not shown). We next examined the dose-dependence by adding 0.5, 1, 5, 10, 50 μM of the 18 compounds. Among them, verapamil, a calcium channel blockers, showed the most consistent and promising dose-dependent activation of the *FRZB* promoter activity and can be used for a long time without major adverse effects (Figure 1A). We also found that verapamil suppressed the Wnt/β-catenin activity in a dose-dependent manner (Figure 1B). Verapamil is an L-type calcium channel blocker that has long been used for hypertension, angina pectoris, cardiac arrhythmia, and most recently cluster headache [23]. We also examined seven other calcium channel blockers (nifedipine, thioridazine, diltiazem, loperamide, perhexiline, nicardipine, felopdipine), but none had an effect (data not shown).

Verapamil upregulates native FRZB and induces expressions of chondrogenic genes in osteoarthritic chondrocyte (OAC) cells

In OA, breakdown of the extracellular matrix around chondrocytes leads to progressive destruction of articular structures [24]. To investigate the effect of verapamil on human OAC cells, we isolated OAC cells from patients with severe OA undergoing total knee replacement surgery. We first confirmed that verapamil upregulated the native FRZB at the mRNA and protein levels (Figure 2A). We screened signaling pathways that were potentially activated by verapamil to facilitate upregulation of FRZB, but found none (Figure S2).

Verapamil also upregulated mRNAs for *ACAN* encoding aggrecan, *COL2A1* encoding collagen type II α1, and *SOX9* encoding SRY-box 9 in a dose-dependent manner (Figure 2B). We next confirmed in OAC cells that Wnt3A upregulated *AXIN2* mRNA, a specific marker of Wnt/β-catenin signaling [25] and *MMP3* mRNA, a gene encoding catabolic metalloproteinase 3 (Figure 2C). As expected, verapamil suppressed *AXIN2* and *MMP3* in a dose-dependent manner (Figure 2D). We additionally observed that verapamil suppressed Wnt3A-mediated expression of total cellular β-catenin (Figure 3A), and nuclear translocation of β-catenin (Figure 3B).

LiCl is an inhibitor of Gsk3β and activates Wnt/β-catenin signaling. As expected, verapamil had no effects on LiCl-induced upregulations of *AXIN2* and *MMP3* in OAC cells (Figure 2E), whereas knocking down of *FRZB* cancelled the effects of verapamil (Figure 2F). These results underscored a notion that verapamil upregulates expression of FRZB and downregulates Wnt/β-catenin signaling in OAC cells.

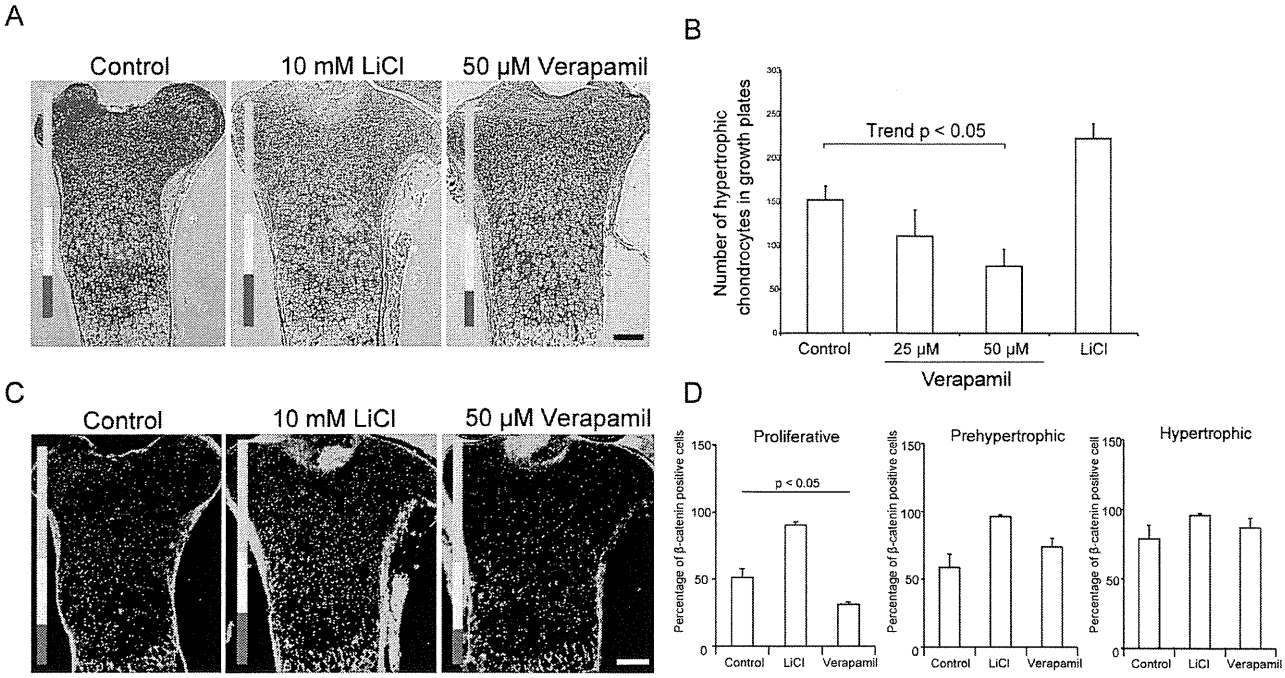

Figure 4. Verapamil suppresses hypertrophic differentiation of chondrocytes and β-catenin staining in growth plates in explanted mouse fetal tibiae on embryonic day 17.5. (A) Tibiae are cultured with LiCl or verapamil for 10 days, and coronal slices of paraffin sections are stained with Alcian blue combined with hematoxylin and eosin staining. Three layers of proliferative (green), prehypertrophic (yellow), and hypertrophic (red) zones are indicated by bars. Scale bar = 200 μm. (B) Verapamil suppresses the number of chondrocytes in the hypertrophic zone in (A). (C) Immunofluorescence with antibody against β-catenin in proximal tibiae of mouse embryo (E17.5). Color bars indicate layers as indicated in (A). Scale bar = 200 μm. (D) Verapamil suppresses the number of β-catenin-positive cells in the proliferative zone. The mean and SEM ($n = 3$) are indicated. *$p<0.05$ versus control by one-way ANOVA with Tukey's test.
doi:10.1371/journal.pone.0092699.g004

Verapamil rescues Wnt3A-induced degradation of proteoglycans in differentiated ATDC5 cells

Chondrocytes produce and maintain the cartilaginous matrix, which is mostly comprised of collagens and proteoglycans [7]. To investigate the effects of verapamil on degradation of proteoglycans, we performed Alcian blue staining to quantify acidic polysaccharides, such as glycosaminoglycans, in differentiated mouse chondrogenic ATDC5 cells. As OAC cells were not able to produce an appreciable amount of proteoglycans (data not shown), we used chondrogenically differentiated ATDC5 cells. We found that Wnt3A treatment induced loss of proteoglycans in ATDC5 cells and verapamil rescued the loss in a dose-dependent manner (Figure 3C).

Verapamil suppresses hypertrophic differentiation of chondrocytes in growth plates

Differentiation of chondrocytes including endochondral ossification is essential for embryonic skeletal growth, which has recently been demonstrated to be abnormally operational in development of OA [26]. Wnt/β-catenin signaling facilitates hypertrophic differentiation of chondrocytes in embryonic growth plates [27]. To investigate the effects of verapamil on hypertrophic differentiation of chondrocytes in growth plates, we cultured explanted mouse fetal tibiae with verapamil. We also treated the explanted tibiae with LiCl to confirm the responsiveness to Wnt/β-catenin. Verapamil had no gross effects on the metaphysis and diaphysis. Zonal analysis of the proximal growth plates showed that LiCl increased and verapamil decreased the height of the hypertrophic zone (Figure 4A). The numbers of hypertrophic chondrocytes counted by two blinded observers also underscored LiCl-mediated enhancement and verapamil-mediated suppression of the hypertrophic zone (Figure 4B). Immunostaining of β-catenin also showed that verapamil inhibited accumulation of β-catenin in growth plates, especially in the proliferative zone (Figures 4C and 4D). These results suggest that verapamil has an inhibitory effect on hypertrophic differentiation of chondrocytes in growth plates.

Verapamil ameliorates OA in a rat model

ure 5C). These results indicate that verapamil inhibits Wnt signaling and ameliorates progression of OA *in vivo*.

Discussion

In physiological endochondral ossification, chondrocytes become hypertrophic and remove the extracellular matrix proteins by expressing MMPs and ADMTSs. Chondrocytes finally die by apoptosis and are substituted by osteoblasts [28,29]. Recent studies disclose that OA follow a similar path to the physiological endochondral ossification: chondrocytes lose the stable phenotype and undergo terminal differentiations, as indicated by upregulation of marker genes for hypertrophy [26]. Wnt/β-catenin signaling pathway is known to drive endochondral ossifications by upregulating MMPs and ADAMTSs [30] in both physiological and pathological conditions [8]. Homeostasis of cartilage in adults is thus maintained by suppressed Wnt/β-catenin signaling, which is exemplified by the fact that FRZB functions as a natural brake to hypertrophic differentiation of chondrocytes [17]. Here we investigated the effects of verapamil on development and progression of OA, and revealed that verapamil (i) enhances

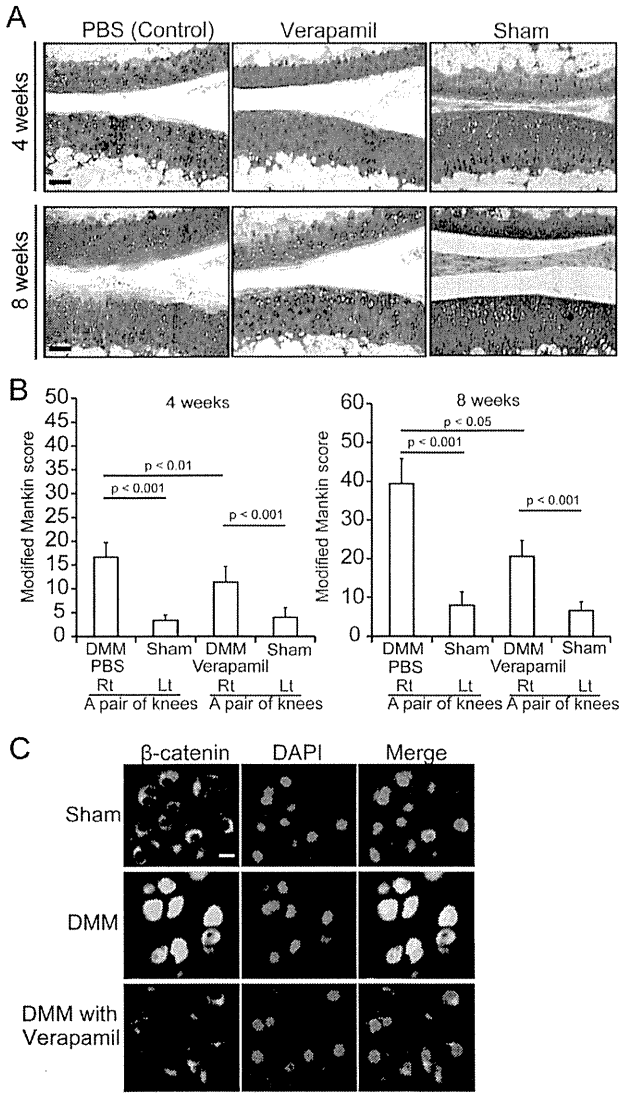

Figure 5. Verapamil prevents OA progression and β-catenin accumulation in rat DMM model. (A, B) DMM surgery induces mild OA phenotype in Wistar/ST rat and verapamil prevents OA progression. (A) Representative staining of knee joints with Safranin O and fast green. Scale bars = 200 μm. (B) Verapamil suppresses OA progressions evaluated by modified Mankin score at four and eight weeks after the surgery. Three rats in each group had DMM and sham surgeries in the right and left knees, respectively. Mean and SEM ($n = 3$) are indicated. (C) Immunofluorescence staining with anti-β-catenin antibody in rat articular cartilage. Articular chondrocytes at the weight-bearing sites are stained with anti-β-catenin antibody and DAPI. Nuclear translocation of β-catenin in DMM is blocked by verapamil. Scale bar = 20 μm.
doi:10.1371/journal.pone.0092699.g005

FRZB gene expression, (ii) inhibits Wnt/β-catenin signaling, (iii) suppresses ECM degradation, (iv) inhibits hypertrophic differentiation of chondrocytes, and (v) ameliorates OA model rats. We used up to 50 μM verapamil *in vitro* (Figure 1), *ex vivo* (Figure 4), and *in vivo* (Figure 5) without overt adverse effects, although the feasibility of intraarticular injection of 50 μM verapamil in clinical practice needs to be carefully validated.

In addition to FRZB, verapamil upregulates another chondrogenic key gene, *SOX9* (Figure 2B). SOX9 is a transcriptional factor that drives chondrogenic differentiation including upregulation of *COL2A1* [31], and is a physiological inhibitor against hypertrophic conversion of chondrocytes in growth plates [32]. Interestingly, physiological binding of SOX9 and β-catenin degrades both SOX9 and β-catenin, which indicates that activated Wnt/β-catenin degrades SOX9 and vice versa [33]. Verapamil is thus expected to increase the amount of SOX9 by suppressing Wnt/β-catenin. This mechanism is likely to account for the verapamil-mediated upregulation of *SOX9* transcripts (Figure 2B), because SOX9 protein upregulates expression of *SOX9* mRNA by forming a positive feedback loop [34].

As stated in the introduction, activation of Wnt/β-catenin worsens OA [7-11] and its inhibition ameliorates OA [12–14,17]. In contrast, however, constitutive inhibition of β-catenin in chondrocytes also leads to OA in mice [35]. Additionally, another Wnt antagonist, DKK1, promotes secretion of matrix proteinases in synovial fibroblasts and accelerates cartilage destruction [36]. These reports suggest that excessive suppression of Wnt/β-catenin may be rather deleterious in OA. The intraarticular administration of a high concentration of verapamil was likely to have suppressed Wnt/β-catenin signaling moderately and exerted beneficial effects in our rat model of OA.

The ATP-binding cassette (ABC) transporter exports hyaluronan to the extracellular matrix space [37] and hyaluronan is abnormally overproduced in OA cartilage [38]. As multidrug resistance (MDR) inhibitors including verapamil inhibits the ABC transporter [39], verapamil was intraarticularly injected in a rat OA model and verapamil indeed prevented abnormal production of hyaluronan and loss of aggrecan in osteoarthritic rat knees [40]. We observed a similar effect of verapamil on OA and have shown that the effects are mediated by upregulation of FRZB. Wnt/β-catenin signaling upregulates the ABC transporter in cerebral endothelium [41] and cancerous cells [42]. Although Wnt-mediated upregulation of the ABC transporter has not been reported in chondrocytes to our knowledge, suppression of the ABC transporter is likely to be another target of FRZB. As verapamil was approved as a class IV antiarrhythmic agent by FDA and has long been used without major adverse effects, verapamil holds promise as a therapeutic option for patients suffering from OA.

Supporting Information

Figure S1 Representative low magnification images of articular surfaces of rat knees after DMM surgery shown in Fig. 5A (boxed). Sections are stained with Safranin O and fast green. Scale bars = 500 μm.
(TIF)

Figure S2 Firefly luciferase activity for *FRZB* promoter in HCS cells treated with verapamil alone or in the presense of inhibitor of other signaling molecules. There are no significant difference between control and each group. Mean and SEM ($n = 8$) are indicated.
(EPS)

Acknowledgments

We would like to thank Dr. Masaharu Takigawa for providing HCS-2/8 cells.

Author Contributions

Conceived and designed the experiments: AT BO NI KO. Performed the experiments: AT. Analyzed the data: AT BO. Contributed reagents/materials/analysis tools: AT BO MI AM TS. Wrote the paper: AT BO KO.

References

1. Hunter DJ, Felson DT (2006) Osteoarthritis. BMJ 332: 639–642.
2. Lawrence RC, Felson DT, Helmick CG, Arnold LM, Choi H, et al. (2008) Estimates of the prevalence of arthritis and other rheumatic conditions in the United States. Part II. Arthritis Rheum 58: 26–35.
3. Kamekura S, Hoshi K, Shimoaka T, Chung U, Chikuda H, et al. (2005) Osteoarthritis development in novel experimental mouse models induced by knee joint instability. Osteoarthritis Cartilage 13: 632–641.
4. De Luca F, Barnes KM, Uyeda JA, De-Levi S, Abad V, et al. (2001) Regulation of growth plate chondrogenesis by bone morphogenetic protein-2. Endocrinology 142: 430–436.
5. Vortkamp A, Lee K, Lanske B, Segre GV, Kronenberg HM, et al. (1996) Regulation of rate of cartilage differentiation by Indian hedgehog and PTH-related protein. Science 273: 613–622.
6. Stewart AJ, Houston B, Farquharson C (2006) Elevated expression of hypoxia inducible factor-2alpha in terminally differentiating growth plate chondrocytes. J Cell Physiol 206: 435–440.
7. Yuasa T, Otani T, Koike T, Iwamoto M, Enomoto-Iwamoto M (2008) Wnt/beta-catenin signaling stimulates matrix catabolic genes and activity in articular chondrocytes: its possible role in joint degeneration. Lab Invest 88: 264–274.
8. Nalesso G, Sherwood J, Bertrand J, Pap T, Ramachandran M, et al. (2011) WNT-3A modulates articular chondrocyte phenotype by activating both canonical and noncanonical pathways. J Cell Biol 193: 551–564.
9. Thomas RS, Clarke AR, Duance VC, Blain EJ (2011) Effects of Wnt3A and mechanical load on cartilage chondrocyte homeostasis. Arthritis Res Ther 13: R203.
10. Zhu M, Tang D, Wu Q, Hao S, Chen M, et al. (2009) Activation of beta-catenin signaling in articular chondrocytes leads to osteoarthritis-like phenotype in adult beta-catenin conditional activation mice. J Bone Miner Res 24: 12–21.
11. Hwang SG, Yu SS, Ryu JH, Jeon HB, Yoo YJ, et al. (2005) Regulation of beta-catenin signaling and maintenance of chondrocyte differentiation by ubiquitin-independent proteasomal degradation of alpha-catenin. J Biol Chem 280: 12758–12765.
12. Lories RJ, Peeters J, Bakker A, Tylzanowski P, Derese I, et al. (2007) Articular cartilage and biomechanical properties of the long bones in Frzb-knockout mice. Arthritis Rheum 56: 4095–4103.
13. Lane NE, Nevitt MC, Lui LY, de Leon P, Corr M, et al. (2007) Wnt signaling antagonists are potential prognostic biomarkers for the progression of radiographic hip osteoarthritis in elderly Caucasian women. Arthritis Rheum 56: 3319–3325.
14. Chan BY, Fuller ES, Russell AK, Smith SM, Smith MM, et al. (2011) Increased chondrocyte sclerostin may protect against cartilage degradation in osteoarthritis. Osteoarthritis Cartilage 19: 874–885.
15. Hoang B, Moos M Jr, Vukicevic S, Luyten FP (1996) Primary structure and tissue distribution of FRZB, a novel protein related to Drosophila frizzled, suggest a role in skeletal morphogenesis. J Biol Chem 271: 26131–26137.
16. Loughlin J, Dowling B, Chapman K, Marcelline L, Mustafa Z, et al. (2004) Functional variants within the secreted frizzled-related protein 3 gene are associated with hip osteoarthritis in females. Proc Natl Acad Sci U S A 101: 9757–9762.
17. Leijten JC, Emons J, Sticht C, van Gool S, Decker E, et al. (2012) Gremlin 1, frizzled-related protein, and Dkk-1 are key regulators of human articular cartilage homeostasis. Arthritis Rheum 64: 3302–3312.
18. Abbott A (2002) Neurologists strike gold in drug screen effort. Nature 417: 109.
19. Bian Y, Masuda A, Matsuura T, Ito M, Okushin K, et al. (2009) Tannic acid facilitates expression of the polypyrimidine tract binding protein and alleviates deleterious inclusion of CHRNA1 exon P3A due to an hnRNP H-disrupting mutation in congenital myasthenic syndrome. Hum Mol Genet 18: 1229–1237.
20. Takigawa M, Tajima K, Pan HO, Enomoto M, Kinoshita A, et al. (1989) Establishment of a clonal human chondrosarcoma cell line with cartilage phenotypes. Cancer Res 49: 3996–4002.
21. Mankin HJ, Dorfman H, Lippiello L, Zarins A (1971) Biochemical and metabolic abnormalities in articular cartilage from osteo-arthritic human hips. II. Correlation of morphology with biochemical and metabolic data. J Bone Joint Surg Am 53: 523–537.
22. Furman BD, Strand J, Hembree WC, Ward BD, Guilak F, et al. (2007) Joint degeneration following closed intraarticular fracture in the mouse knee: a model of posttraumatic arthritis. J Orthop Res 25: 578–592.
23. Beck E, Sieber WJ, Trejo R (2005) Management of cluster headache. Am Fam Physician 71: 717–724.
24. Little CB, Fosang AJ (2010) Is cartilage matrix breakdown an appropriate therapeutic target in osteoarthritis–insights from studies of aggrecan and collagen proteolysis? Curr Drug Targets 11: 561–575.
25. Jho EH, Zhang T, Domon C, Joo CK, Freund JN, et al. (2002) Wnt/beta-catenin/Tcf signaling induces the transcription of Axin2, a negative regulator of the signaling pathway. Mol Cell Biol 22: 1172–1183.
26. Saito T, Fukai A, Mabuchi A, Ikeda T, Yano F, et al. (2010) Transcriptional regulation of endochondral ossification by HIF-2alpha during skeletal growth and osteoarthritis development. Nat Med 16: 678–686.
27. Hens JR, Wilson KM, Dann P, Chen X, Horowitz MC, et al. (2005) TOPGAL mice show that the canonical Wnt signaling pathway is active during bone development and growth and is activated by mechanical loading in vitro. J Bone Miner Res 20: 1103–1113.
28. Wang Y, Middleton F, Horton JA, Reichel L, Farnum CE, et al. (2004) Microarray analysis of proliferative and hypertrophic growth plate zones identifies differentiation markers and signal pathways. Bone 35: 1273–1293.
29. Inada M, Wang Y, Byrne MH, Rahman MU, Miyaura C, et al. (2004) Critical roles for collagenase-3 (Mmp13) in development of growth plate cartilage and in endochondral ossification. Proc Natl Acad Sci U S A 101: 17192–17197.
30. Ryu JH, Kim SJ, Kim SH, Oh CD, Hwang SG, et al. (2002) Regulation of the chondrocyte phenotype by beta-catenin. Development 129: 5541–5550.
31. Lefebvre V, Li P, de Crombrugghe B (1998) A new long form of Sox5 (L-Sox5), Sox6 and Sox9 are coexpressed in chondrogenesis and cooperatively activate the type II collagen gene. EMBO J 17: 5718–5733.
32. Akiyama H, Chaboissier MC, Martin JF, Schedl A, de Crombrugghe B (2002) The transcription factor Sox9 has essential roles in successive steps of the chondrocyte differentiation pathway and is required for expression of Sox5 and Sox6. Genes Dev 16: 2813–2828.
33. Akiyama H, Lyons JP, Mori-Akiyama Y, Yang X, Zhang R, et al. (2004) Interactions between Sox9 and beta-catenin control chondrocyte differentiation. Genes Dev 18: 1072–1087.
34. Kumar D, Lassar AB (2009) The transcriptional activity of Sox9 in chondrocytes is regulated by RhoA signaling and actin polymerization. Mol Cell Biol 29: 4262–4273.
35. Zhu M, Chen M, Zuscik M, Wu Q, Wang YJ, et al. (2008) Inhibition of beta-catenin signaling in articular chondrocytes results in articular cartilage destruction. Arthritis Rheum 58: 2053–2064.
36. Weng LH, Ko JY, Wang CJ, Sun YC, Wang FS (2012) Dkk-1 promotes angiogenic responses and cartilage matrix proteinase secretion in synovial fibroblasts from osteoarthritic joints. Arthritis Rheum 64: 3267–3277.
37. Ouskova G, Spellerberg B, Prehm P (2004) Hyaluronan release from Streptococcus pyogenes: export by an ABC transporter. Glycobiology 14: 931–938.
38. Hamerman D, Sasse J, Klagsbrun M (1986) A cartilage-derived growth factor enhances hyaluronate synthesis and diminishes sulfated glycosaminoglycan synthesis in chondrocytes. J Cell Physiol 127: 317–322.
39. Prehm P, Schumacher U (2004) Inhibition of hyaluronan export from human fibroblasts by inhibitors of multidrug resistance transporters. Biochem Pharmacol 68: 1401–1410.
40. Prehm P (2005) Inhibitors of hyaluronan export prevent proteoglycan loss from osteoarthritic cartilage. J Rheumatol 32: 690–696.
41. Strazielle N, Ghersi-Egea JF (2013) Physiology of blood-brain interfaces in relation to brain disposition of small compounds and macromolecules. Molecular pharmaceutics 10: 1473–1491.
42. Correa S, Binato R, Du Rocher B, Castelo-Branco MT, Pizzatti L, et al. (2012) Wnt/beta-catenin pathway regulates ABCB1 transcription in chronic myeloid leukemia. BMC cancer 12: 303.

Intronic and Exonic Nucleotide Variations that Affect RNA Splicing in Humans

Kenji Ohe, Akio Masuda and Kinji Ohno
Division of Neurogenetics, Center for Neurological Diseases and Cancer
Nagoya University Graduate School of Medicine, Nagoya, Japan

1 Introduction

Identification of the 3.2 billion nucleotides of the human genome, the human genome project, and the gene annotation projects thereafter have revealed that human has merely 22,000-25,000 protein coding genes. Comparison with other genomes has highlighted the significance of a higher degree of alternative splicing in human to produce the vast proteome compared to other species. During the millions of years of evolution, our genome has been extensively mutated and exposed to natural selection. Ten percent of mutations, which cause hereditary disease, disrupt the splice site consensus sequence at the 5' splice site and 3' splice site (Krawczak *et al.*, 2007). Indeed, 11,525 splicing mutations out of 123,656 total mutations are registered in the Human Genome Mutation Database (HGMD) professional release 2012.1 (http://www.hgmd.org/). Splicing, however, does not only rely on the splice site consensus sequences. Considering auxiliary splicing *cis*-elements along with the recent advances in resequencing technologies of the human genome, the rate of disease-causing mutations affecting splicing has been estimated to be up to 60% (Hammond&Wood, 2011). Studying the mechanisms of splicing disruption will elucidate the molecular bases of development of disease and also give us essential information on how and why the human genome has evolved.

Mechanisms of splicing disruption can be categorized into three groups: a) disruption of splicing *cis*-element; b) aberrant expression or abnormal function of splicing *trans*-factors; and c) RNA gain-of-function disorders, in which a splicing *trans*-factor is sequestered to abnormally expanded RNA repeats and forms an abnormal aggregate. Abnormal expression of splicing *trans*-factors is observed in various types of cancer, in which SRSF1 (ASF/SF2) is an oncogenic product (Karni *et al.*, 2007). Another example of an abnormally regulated *trans*-factor is the oncogenic product HMGA1a (HMG I/Y), which binds upstream of the 5' splice site and traps U1 snRNP at the 5' splice site (Ohe&Mayeda, 2010) and results in aberrant alternative splicing of *PSEN2* encoding presenilin-2 in sporadic Alzheimer's disease (Manabe *et al.*, 2003). RNA gain-of-function mechanisms are observed in neurological disorders including myotonic dystrophy, spinocerebellar ataxia, and paraneoplastic syndromes (Licatalosi&Darnell, 2006; O'Rourke&Swanson, 2009). This chapter is dedicated to disruption of intronic and exonic splicing *cis*-elements. Please refer to other review articles for other abnormal splicing mechanisms (Licatalosi&Darnell, 2006; O'Rourke&Swanson, 2009; Ohno K, 2011).

Splicing occurs as a two-step *trans*-esterification reaction after the step-wise assembly of uridine-rich small nuclear ribonucleoproteins (U snRNPs) of the spliceosome (Smith *et al.*, 2008; Wahl *et al.*, 2009) (Figure 1A). Though the average length of human introns is more than 3,300 nucleotides (Lander *et al.*, 2001), variation in length is immense; from a 43-nucleotide intron in *ESRP2* (epithelial splicing regulatory protein 2) (Sasaki-Haraguchi *et al.*, 2012) to a 740,920-nucleotide intron found in the heparan sulfate 6-O-sulfotransferase 3 gene (Fedorova&Fedorov, 2005). Thus, in higher eukaryotes, splicing is mostly defined by exon rather than intron (Figure 1B) (Berget, 1995). Using this exon definition model, a number of algorithms have been developed to give a probable answer on the consequence of a single nucleotide variation (SNV). No algorithm, however, is 100% accurate. Splicing consequences should be tested with a combination of different algorithms and should be verified by splicing substrates *in vitro* and/or *in vivo*.

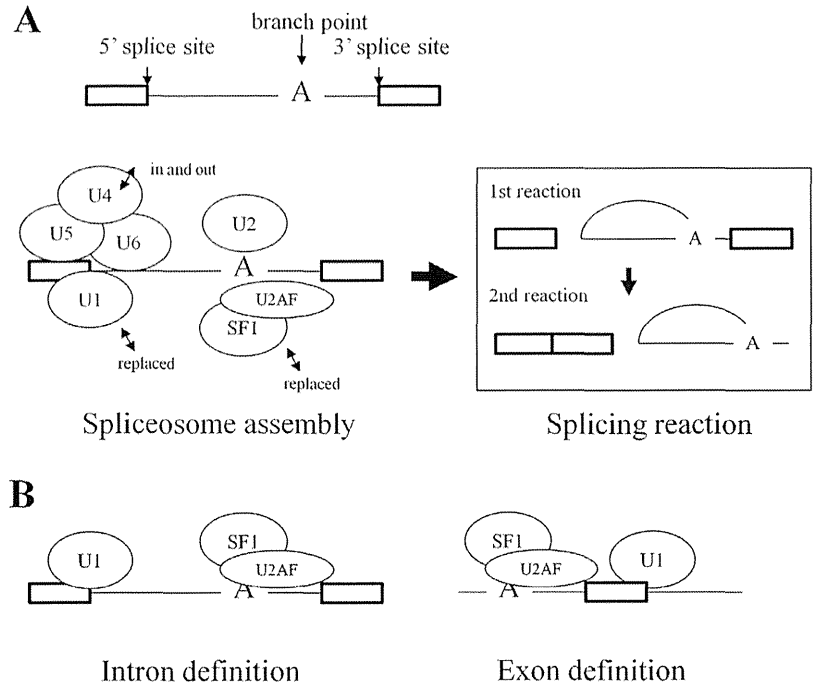

Figure 1: A, Assembly of the spliceosome by U snRNPs and associated factors (left) and the two-step *trans*-esterification reaction after the assembly of the spliceosome (right). **B,** The intron definition model for lower eukaryotes and exon definition model for higher eukaryotes. U1-6, U1-6 snRNP; SF1, splicing factor 1; U2AF, U2 snRNP auxiliary factor.

2 Intronic nucleotide variations

2.1 Intronic splicing *cis*-elements

In eukaryotes, pre-mRNA splicing is conducted by essential nucleotide sequences on the splicing substrate (*cis*-elements) and *trans*-factors that bind to these sequences. Core *cis*-elements involve the 5' splice site, the branch point sequence (BPS), polypyrimidine tract (PPT) and the 3' splice site, to which the *trans*-factors, U1 small nuclear ribonucleoprotein (U1 snRNP), SF1/mBBP and later U2 small nuclear ribonucleoprotein (U2 snRNP), U2 snRNP auxiliary factor 65 (U2AF65), and U2 snRNP auxiliary factor 35 (U2AF35) associate, respectively (Figure 1A). Besides these classical *cis*-elements, a growing number of intronic splicing enhancer/silencer (ISE, ISS) are known to function in alternative splicing, which, however, are difficult to predict from the nucleotide sequence alone. The tissue- and development-specific expression of these *trans*-factors that recognize these *cis*-elements makes the fine-tuned alternative splicing possible.

2.1.1 5' splice site

The consensus sequence of the 5' splice site is "CAG/GUAAGUAU", where "/" indicates an exon-intron boundary (Lerner *et al.*, 1980; Roca&Krainer, 2009). Several computational methods have been developed to evaluate the 5' splice site including the Shapiro and Senapathy matrix (Shapiro&Senapathy, 1987), the weight matrix model (Staden, 1984), the first-order Markov model (Salzberg, 1997), the max-

imum dependence decomposition model (Burge&Karlin, 1997), and the maximum entropy model (Yeo&Burge, 2004). Many reports have been made on aberrant splicing due to disease-associated SNVs at the 5' splice site. The computational methods above are optimized for evaluating the strength of U1 snRNP-binding to the 5' splice site, but are not designed for evaluating the effect of an SNV on aberrant splicing. Algorithms to predict an activated cryptic 5' splice site due to an SNV at the 5' splice site have been created: an EST-based method called Cryptic Splice Finder (Kapustin *et al.*, 2011), which uses the information content of nucleotide frequencies at each 5' splice site (Rogan *et al.*, 1998; Nalla&Rogan, 2005). Calculation of free energy for stable binding of U1 snRNA to the 5' splice site has also been proposed (ΔG) (Roca *et al.*, 2005). More recently, a structure-based method, the structure profiles and odds measure (SPO algorithm), was developed for identifying cryptic 5' splice sites (Tsai&Wang, 2012). In order to predict a splicing consequence of an SNV at the 5' splice site, we have also analyzed splicing patterns of 31 mini-genes carrying naturally occurring or artificially introduced mutations at various nucleotides of the 5' splice site using a cell culture system (Sahashi *et al.*, 2007). We found that a new parameter, the SD-score, efficiently predicts the splicing consequences of SNVs at the 5' splice site. SD-score is a common logarithm of the frequency in the human genome of a specific 9-nucleotide sequence spanning 3 nucleotides at the 3' end of an exon and 6 nucleotides at the 5' end of an intron. The SD-score predicted the splicing consequences of the 31 mini-genes and 179 reported SNVs at the 5' splice site with the sensitivity of 97.1 % and specificity of 94.7 %. We simulated all possible SNVs at 189,249 5' splice sites in the human genome using this SD-score, and found that 37.8%, 88.8%, 96.8%, 82.8%, 95.0%, 96.5%, and 63.0% of SNVs at exonic positions -3, -2, -1, and intronic position +3, +4, +5, +6, respectively, were predicted to cause aberrant splicing, which were all higher than we expected. Using the SD-score we indeed detected four mutations at the 5' splice site causing aberrant splicing, which have been overlooked. The SD-score web service program is available at http://www.med.nagoya-u.ac.jp/neurogenetics/SD_Score/sd_score.html.

A problem shared by these computational methods is that they rely on prediction of binding of U1 snRNP to the 5' splice site. The problem emerges at the non-canonical 5' splice sites: 0.9% of 5' splice sites carry GC dinucleotide and 0.36% harbor U12-type 5' splice sites with AT dinucleotide (Sheth *et al.*, 2006). Also it has been reported that base pairing is shifted by one nucleotide between the 5' splice site and U1 snRNA at 59 5' splice sites (Roca&Krainer, 2009). A subsequent report shows that as much as ~5% of 5' splice sites are recognized by U1 snRNA by bulged nucleotides on either the 5' splice site or U1 snRNA (Roca *et al.*, 2012).

2.1.2 Human branch point sequence (BPS)

Yeast carries a strictly conserved BPS of "UACUAAC" (Langford&Gallwitz, 1983). In eukaryotes, however, the BPS had not been evaluated through global experimental verification. Previously reported consensus sequences of eukaryote BPS were either based on analyses of only a few experimentally identified branch points or *in silico* search for sequences which resemble the yeast consensus BPS.

As depletion of SF1 does not abrogate splicing in HeLa nuclear extract, SF1 may be dispensable in most pre-mRNAs (Tanackovic&Kramer, 2005). An SF-1 affinity model, in which validated SF1 affinity data is employed, efficiently predicts BPS in putative SF1-dependent introns (Pastuszak *et al.*, 2011). A computational algorithm for branch point prediction, the SVM-BP finder (http://regulatorygenomics.upf.edu/Software/SVM_BP/), has also been developed (Corvelo *et al.*, 2010). Recently, large-scale sequencing of lariat RT-PCR products determined individual branchpoints in hu-

man pre-mRNAs and also identified 66 disrupted branchpoints associated with human diseases (Taggart *et al.*, 2012).

Development of lariat RT-PCR has markedly increased efficiency of identifying BPSs (Vogel *et al.*, 1997). We conducted lariat RT-PCR of 52 introns of 20 housekeeping genes. Analysis of 367 lariat RT-PCR clones disclosed that the human consensus BPS is "yUnAy" (y, pyrimidine; n, any nucleotide) (Gao *et al.*, 2008). The fourth nucleotide "A" is the branchpoint (position +0) and is conserved in 92.3% of the clones. The "U" at position -2 is conserved in 74.6%. Collation of 46 experimentally verified BPSs that have been previously published also resulted in a "yUnAy" sequence.

2.1.3 3' splice site

The 3' splice site consists of 3' end of an intron and 5' end of an exon, having a consensus sequence of "NYAG/R" (N, any nucleotide; Y, pyrimidine; R, purine; "/", intron-exon boundary) (Zhang, 1998). U2AF35 binds to this sequence at early steps of the splicing reaction. At later steps, the dinucleotide "AG" is scanned downstream of the branchpoint and the first "AG" is recognized as the 3' end of the intron, "AG scanning model" (Smith *et al.*, 1989). SNVs of this kind have been reported; an 18-nucleotide duplication comprising 16 intronic and 2 exonic residues of the *HEXB* gene encoding the β subunit of β-hexosaminidase results in an active upstream copy of the 3' splice sites (Dlott *et al.*, 1990). A 69-nucleotide duplication comprising 7 intronic and 62 exonic residues of *SLC4A1* encoding anion exchanger member 1 also results in an active upstream copy of the 3' splice sites (Bianchi *et al.*, 1997). We have characterized a mutation of this kind in a patient with congenital myasthenic syndrome. The mutation was a duplicated sequence of 16 nucleotides at the junction of intron 10 and exon 11 of the acetylcholine receptor ε subunit gene (*CHRNE*) (Ohno *et al.*, 2005). The upstream of the duplicated "AG" was always recognized and generated aberrant protein.

On the contrary, a mutation of the *BTD* gene encoding biotinidase creates a downstream 3' splice site with a stronger polypyrimidine tract which results in usage of the downstream AG, not following the AG scanning model (Pomponio *et al.*, 1997). Analyses of the β-globin gene in β-thalassemia patients (Spritz *et al.*, 1981; Westaway&Williamson, 1981; Metherall *et al.*, 1986) and deletion mutagenesis analyses of the rabbit β-globin intron 2 have disclosed the following rule. When the upstream cryptic 3' splice site is more than 24 nucleotides away from the authentic 3' splice site, the authentic 3' splice site is used; less than 21 nucleotides, the cryptic 3' splice site is used; between 21 and 24 nucleotides, both cryptic and authentic 3' splice sites are used (Chua&Reed, 2001; Wieringa *et al.*, 1984). A chromatin- and RNA-associated protein, DEK, facilitates the U2AF35-AG interaction and prevents binding of U2AF65 to pyrimidine tracts not followed by AG (Soares *et al.*, 2006). As described later, hnRNPA1 also discriminates authentic 3' splice sites from pyrimidine-rich RNA segments by recognizing AG at the 3' end of an intron (Tavanez *et al.*, 2012).

Extensive mutational analyses of nucleotides surrounding the 3' splice site of *FAS* revealed that, though U2AF35-binding sequences are highly degenerative, the auxiliary nucleotides are essential for binding of U2AF35 (Corrionero *et al.*, 2011).

Recent analysis of large-scale mapping of the human branchpoints has revealed 80% of the branchpoints follow the AG scanning model. A decision tree optimized by the ID3 algorithm was developed for AG selection to an accuracy of 95.5%. This decision tree includes four steps: 1) whether the AG of interest is the first one after the branchpoint or not, 2) whether the first AG is more than 7 nucleotides downstream the branchpoint or not, 3) whether the distance between the first and next AG is more than

14 nucleotides or not, 4) if the AG decided is within an optimal range from the branchpoint (16-25 nucleotides) (Taggart *et al.*, 2012).

2.1.4 Intronic splicing enhancers (ISE) / intronic splicing silencers (ISS)

In human, prediction of disruption of intronic *cis*-elements would be more difficult than exonic *cis*-elements due to the fact that introns are much longer than exons. Many examples of aberrant activation of pseudo-exons due to mutations have been documented (Dhir&Buratti, 2010). Most of these pseudo-exons originate from transposable elements that make up half of the human genome (Vorechovsky, 2010). They are likely to be suppressed by nucleotide substitutions acquired in the course of evolution (Schmitz&Brosius, 2011), and are reactivated by a disease-causing mutation. Currently available exon scanning tools cannot fully predict aberrant activation due to these mutations. We thus have listed the position in gene and resulting disease in Table 1, with the hope of assisting development of an accurate algorithm which predicts exonization due to an intronic SNV and for aid of the development of the recent antisense therapies which correct expression of these pseudo-exons (Wood *et al.*, 2007) especially in neuromuscular disorders (Wood *et al.*, 2010).

The average length of these 124 pseudo-exons identified in 61 diseases is 109 nucleotides, which is slightly shorter than the average size of human exons of 126 nucleotides (Schwartz *et al.*, 2009). Recently disclosed link of histone modifications (Kolasinska-Zwierz *et al.*, 2009) and nucleosome (Beckmann&Trifonov, 1991; Tilgner *et al.*, 2009) to alternative splicing has led to speculation that 120 bp of DNA wrapping a subnucleosome structure, the $(H3\text{-}H4)_2$ histone tetramer, is protected from nucleotide substitutions and marks the exon for the splicing machinery in higher eukaryotes (Keren *et al.*, 2010). The growing list of aberrantly activated pseudo-exons predicts that intronic mutations causing abnormal splicing are more involved in disease mechanisms than have been previously expected. Indeed, the frequency of these types of mutations has been calculated up to 7% in some diseases (Pros *et al.*, 2009; Gurvich *et al.*, 2008).

We have also identified a G-to-A mutation at 8 nucleotides upstream the 3' end of intron 3 (IVS3-8G>A) of the *CHRNA1* gene. In this patient, a missense mutation that decreases the expression of acetylcholine receptor was also identified on one allele, and the IVS3-8G>A mutation was found on the other. We thus checked splicing products in the patient's biopsied muscle and found that an alternative exon P3A downstream of exon 3 is exclusively activated by IVS3-8G>A. As the mutation does not disrupt any known splicing *cis*-element, we sought for a responsible splicing *trans*-factor and identified that hnRNP H binds to this *cis*-element. Biacore surface plasmon resonance (SPR) analysis revealed that the mutation decreases the binding affinity for hnRNP H to 1/100 (Masuda *et al.*, 2008). We also determined polypyrimidine tract binding protein (PTB) as a silencing *trans*-factor for P3A and that tannic acid increases expression of PTB to correct abnormal activation of P3A (Bian *et al.*, 2009).

Disease	**Gene name**	**Size of pseudo-exon and localization**
Afibrinogenemia	*FGB*	50 bp in intron 1
	FGG	75 bp in intron 6
Alport syndrome	*COL4A3*	74 bp in intron 5
	COL4A5	30 bp in intron 29
		147 bp in intron 6

Continued on next page...

...*Continued from previous page*

Amyotrophic lateral sclerosis	*SOD1*	43 bp in intron 4
Ataxia telangiectasia	*ATM*	58 bp in intron 19
		65 bp in intron 20
		112bp in intron 28
		137 bp in intron 40
Autosomal dominant hearing loss	MYO6	108 bp in intron 23
Autosomal dominant retinitis pigmentosa	PRPF31	175 bp in intron 13
Autosomal recessive polycystic kidney disease	PKHD1	116 bp in intron 46
β+ thalassemia	*HBB*	165bp in intron 2
		125 bp in intron 2
		73 bp in intron 2
Breast cancer	*BRCA1*	66 bp in intron 13
	BRCA2	65 bp in intron 16
	ESR1	69 bp in intron 5
Brooke-Spiegler syndrome	*CYLD*	65 bp in intron 9
Choroideremia	*CHM*	98 bp in intron 5
Chronic granulomatous disease	*CYBB*	56 bp in intron 6
		61 bp and 110 bp in intron 5
Congenital cataracts facial dysmorphism neuropathy syndrome	*CTDP1*	95 bp in intron 6
Congenital disorders of glycosylation type Ia	*PMM2*	66 bp in intron 7
		123 bp in intron 7
Chronic myeloid leukemia	*ABL*	35 bp in intron8
	BCR-ABL	42 bp of *ABL* intron 1b
Coagulation factor V deficiency	*F5*	295 bp in intron 8
Cystic fibrosis	*CFTR*	183 bp in intron 3
		101 bp in intron 6
		104 bp in intron 10
		49 bp in intron 11
		214 bp in intron 18
		84 bp in intron 19
DHPR deficiency	*DHPR*	152 bp in intron 3
Duchenne muscular dystrophy	*DMD*	149 bp in intron 1M (Becker type)
		132 and 46 bp in intron 2
		70 bp in intron 4
		90 bp in intron 9 (Becker type)
		in intron 11
		79 bp in intron 11 (Becker type)
		95 bp in intron 25

Continued on next page...

...Continued from previous page

		172 and 202 bp in intron 25
		119 bp in intron 27
		137 bp in intron45
		72 bp in intron 47
		125 bp in intron 48
		108 bp in intron 48
		98 bp in intron 49
		180 bp in intron 49
		160 bp in intron 49
		149 bp in intron 49
		134 bp in intron 56
		89 bp in intron 60 (intermediate type)
		67 bp in intron 62
		58 bp in intron 62
		67 bp in intron 63
		147 bp in intron 65
		53 bp in intron 65
		121 bp in intron 67
Fabry disease	*GLA*	57 bp in intron 4
Familial hemophagocytic lymphohistiocytosis	*UNC13D*	130 bp in intron 1
Fibrochondrogenesis	*COL11A1*	50 bp in intron 48
Fukutin related congenital muscular dystrophy	*FKTN*	64 bp in intron 5
Gitelman's syndrome	*SLC12A3*	238 bp in intron 13 90 bp in intron 21
Globoid-cell leukodystrophy	*GALC*	34 bp in intron 6
Glutathione synthetase deficiency	*GSS*	In exon 2
Growth-hormone insensitivity (Laron syndrome)	*GHR*	108 bp in intron 6
Haemophilia A	*FVIII*	191 bp in intron 1
Holoprosencephaly	*SHH*	129 bp in intron 1
Homocystinuria	*MTRR*	140 bp in intron 6
17α-Hydroxylase Deficiency	*CYP17A1*	95 bp in intron 1
Hyper immunoglobulin M (IgM) syndrome	*CD40L*	59 bp in intron 3
Leber congenital amaurosis	*CEP290*	128 bp in intron 26
Leigh syndrome	*NDUFS7*	122 bp in intron 1
Lynch syndrome	*MSH2*	75 bp in intron 1
Malignant rhabdoid tumor	*SNF5/INI1*	72 bp in intron 1
Maple syrup urine disease	*E2*	126 bp in intron 8
Marfan syndrome	*FBN1*	93 bp in intron 63
Megalencephalic leukoencephalopathy with subcortical cysts	*MLC1*	246 bp in intron 10
3-methylcrotonyl-CoA carboxylase deficiency	*MCBB*	64 bp in intron 10 also deletes exon 11
Methylmalonic acidemia	*MUT*	76 bp in intron 11

Continued on next page...

...Continued from previous page

Mitochondrial trifunctional protein deficiency	*HADHB*	106 and 56 bp in intron7
Mucopolysaccharidosis Type II (Hunter syndrome)	*IDS*	78 bp in intron 7
		103 bp in intron 3
Mucopolysaccharidosis type VII (Sly syndrome)	*GUSB*	68 bp in intron 8
Multiminicore Disease	*RYR1*	119 bp in intron 101
Myopathy with lactic acidosis	*ISCU*	53 bp in intron 4
		86 and 100 bp in intron 5
Neurofibromatosis type 1	*NF-1*	107 bp in intron 3
		58 bp in intron 6
		76 and 54 bp in intron 10
		177 bp in intron 30
		172 bp in intron 30
		70 bp in intron 45
Neurofibromatosis type 2	*NF-2*	106 bp in intron 5
Niemann–Pick type C disease.	*NPC1*	374 bp in intron 1
		108 bp in intron 6
		194 bp in intron 9
Ocular albinism type 1	*OA1*	165 bp in intron7
ornithine δ-aminotransferase deficiency	*OAT*	142 bp in intron 3
Propionic acidemia	*PCCA*	84 bp in intron 14
	PCCB	72 bp in intron 6
Primary ciliary dyskinesia (Kartagener syndrome)	*CCDC39*	116 bp in intron 9
Retinoblastoma	*RB1*	103 bp in intron 23
Schwartz-Jampel syndrome	*HSPG2*	130 bp in intron 6
Tetrahydrobiopterin deficiency	*PTS*	45 bp in intron 2
		79 bp in intron 1
Tuberous sclerosis complex	*TSC2*	89 bp in intron 8
Urea transport deficiency	*JK*	136 bp in intron3 also deletes exon4,5
Usher syndrome type 2	*USH2A*	152 bp in intron 40
X-linked hypophosphatemia	*PHEX*	50, 100, 170 bp in intron 7
		59 bp in intron 19
Werner syndrome	*WRN*	69 bp in intron 25

Table 1: Disease-associated mutations causing aberrant activation of pseudo-exon

3 Exonic nucleotide variations

3.1 Exonic splicing *cis*-elements

3.1.1 First nucleotide of exon

As mentioned above, the consensus 3' splice site is "YAG/G" (Y, pyrimidine). Many SNVs disrupting the AG are known, but few have been reported that disrupt the first nucleotide G in the exon.

We have analyzed the effect of mutations at the first nucleotide in the exon on splicing regulation (Fu *et al.*, 2011). When the length of the pyrimidine stretch of the polypyrimidine tract is longer than 10-15 nucleotides, U2AF65 binds so tight that U2AF35 binding to the YAG/G is dispensable, which is known as the AG-independent splice site. When the pyrimidine stretch is short, U2AF35 needs to bind to the YAG/G for efficient splicing, which is known as the AG-dependent splice site. We have found that when a mutation of the first nucleotide of exon is at an AG-dependent splice site, aberrant splicing occurs, but when a mutation is at an AG-independent splice site, normal splicing takes place. Analyses of 1,796,809 3' splice sites in human revealed that when the first nucleotide of the exon is other than G, the average size of pyrimidine stretches is significantly shorter than that when it is a G. This means that when the 3' splice site is AG-dependent, the probabilities of a short pyrimidine stretch and the first nucleotide of the exon to be a G are higher. We have reported 5 mutations at the first nucleotide of an exon that cause aberrant splicing. The importance of the first nucleotide of an exon is also reported in *FAS* encoding *CD95* gene, in which U2AF35 strictly binds to RCAG/G (R, purine), and is sensitive to a single mutation even at -4, -3, and +1 (Corrionero *et al.*, 2011). Mutations at the first nucleotide of an exon may have been underestimated and attention must be evoked in the field of human genetics.

A total of 20 mutations at the first nucleotide of an exon have been reported: 10 mutations cause aberrant splicing (AS), whereas 10 result in normal splicing (NS) (Table 2). According to our studies (Fu *et al.*, 2011), we can assume that the AS and NS mutations are at the AG-dependent and AG-independent sites, respectively. As expected, all the AS mutations affect a G at the first nucleotide of an exon. We constructed sequence logos using a tool available on-line (Crooks *et al.*, 2004) (http://weblogo.berkeley.edu/logo.cgi) using the 10 AS (Figure 2A) and 10 NS (Figure 2B) mutants. Figure 2A shows that in the 10 AS sites a C at intron -3 is rarely observed. As the consensus sequence for U2AF35 is YAG/G, lack of C at intron -3 makes binding of U2AF35 solely dependent on G at exon +1 in the AS sites. A mutation affecting G at exon +1 thus compromises binding of U2AF35, leading to aberrant splicing. The lengths of uninterrupted stretch of PPT (underlined in Table 2) of the AS and NS sites are 7.4 ± 2.9 and 9.3 ± 4.2 (mean and SD), respectively. Although the difference is not statistically significant, the difference in PPT also suggests that the AS sites are AG-dependent.

Valcarcel and colleagues recently report that U2AF heterodimer requires hnRNPA1 to discriminate *bona fide* 3' splice sites from pyrimidine-rich RNA segments (Tavanez *et al.*, 2012). hnRNP A1 recognizes AG at the 3' end of an intron and facilitates binding of U2AF heterodimer to *bona fide* PPT. As the consensus sequence of hnRNP A1 is "UAGGGW" (W, A or U) (Burd&Dreyfuss, 1994), a G at the first nucleotide of an exon may also be essential for binding to hnRNP A1.

In the course of analysis of mutations at the first nucleotide of an exon, we also found that T is preferentially used at exonic position +3, +4, and +5 in the human genome (Fu *et al.*, 2011). SELEX analysis of U2AF35 also shows that U2AF35 binds up to 12 nucleotides downstream the intron-exon boundary into the exon (Wu *et al.*, 1999). Indeed, preferential usage of T at exonic position +3, +4, +5 is observed in the SELEX dataset. Splicing mutations affecting these thymine nucleotides, however, have not been reported to date.

Mutation at first nucleotide of exon	Gene name /exon	Consequence
Mutations affecting splicing (AG-dependent 3' splice sites to which U2AF35 binds)		
atttaAtttctctgtttttccccttttgtag (G>T)AAGTCACCAAA	*CFTR* / exon 4	Exon skipping, activation of cryptic exon
cacttAcgcattcgtctatctttcgcatag (G>T)TTGGTCCAATG	*FECH* / exon 9	Exon skipping
gactgAtcttgttttctgttccccacag (G>T)GGGTTCCAGCC	*UROS* / exon 9	Exon skipping
gtagAccttggtgggcggtccttctcctag (G>T)AAGAAGCCTAT	*GH1* / exon 3	Exon skipping
tcttcAcctgtcatattcttattttag (G>T)ATCCACCCACT	*EYA1* / exon 12 (previously exon10)	Exon skipping
ccatgAcagaatttaccagaaatgtaaccatctcag (G>T)TCTCTGATGAA	*PKHD1* / exon 25	Exon skipping, activation of cryptic 3' splice site
ctgtaActgtttatttccaacag (G>T) GTGCTGCTGGT	*COL1A2* / exon37	Exon skipping
agatgAcattgccccctggggccttatgtttgggaacacag (G>A)GAGCGCAGAGT	*CLCN2* / exon 19	Exon skipping
ctgtgAccccaaattggtcttcatcctctctctaag (G>T)CTCCATGGTTC	*CAPN3* / exon 5	Exon skipping
atctgAagcatcttcctttctgtttcttctcaag (G>T)TTCCCAAAGAG	*CAPN3* / exon 12	Exon skipping
Mutations not affecting splicing (AG-independent 3' splice sites to which U2AF35 does not bind)		
ttctaAgcagtttacgtgccaattcAatttcttaacctatctcaaag (A>G)TGGAGATCAGT	F9 / exon 4	No effect on splicing
ggcttAtatctgtttattattcAgtattcctgtgtacattttctgtttttatttttatacag (G>del)CTATGTAGAAC	*MSH2* / exon 12	No effect on splicing
gagtgAgtccagggtgcctagacaagaggtagcagcctgtggatgtccagcacctttgcagggaatacagggcccaatctggcacatgccccttttcctccag (G>C)CCCAGAGCAGG	*HEXA* / exon 13	No effect on splicing
aatttAcaaatctgtgttcctgctttttttccctttaag (G>T)CCTCGATCCAG	*LPL* / exon 5	No effect on splicing
ttgtgAtctcttgattttatttcag (G>A)CAAATCCTAAG	*APC* / exon 16	No effect on splicing
ttttaAgtgtttattttcattgactttgcag (A>del)TATTAATGAAT	*FBN1* / exon 20	Predicted to be only amino acid substitution
ctgtaActgtttatttccaacag (G>A)GCCCTCCTGGT	*COL1A2* / exon23	No effect on splicing
ctctgAgggtctcttgtctttcctcag (G>A)TGAATGTGGAA	*LAMA2* / exon 24	No effect on splicing
tgttgAcccttcctcctcccatgacag (G>A)TGCAGCCGCTG	*NEU1* / exon 2	No effect on splicing
cactaAtgcccctctctcctcctgcccccag (G>T)GCGTTCCTGGC	*COL6A2* / exon 8	No effect on splicing

Table 2: Mutations at the first nucleotide of exon

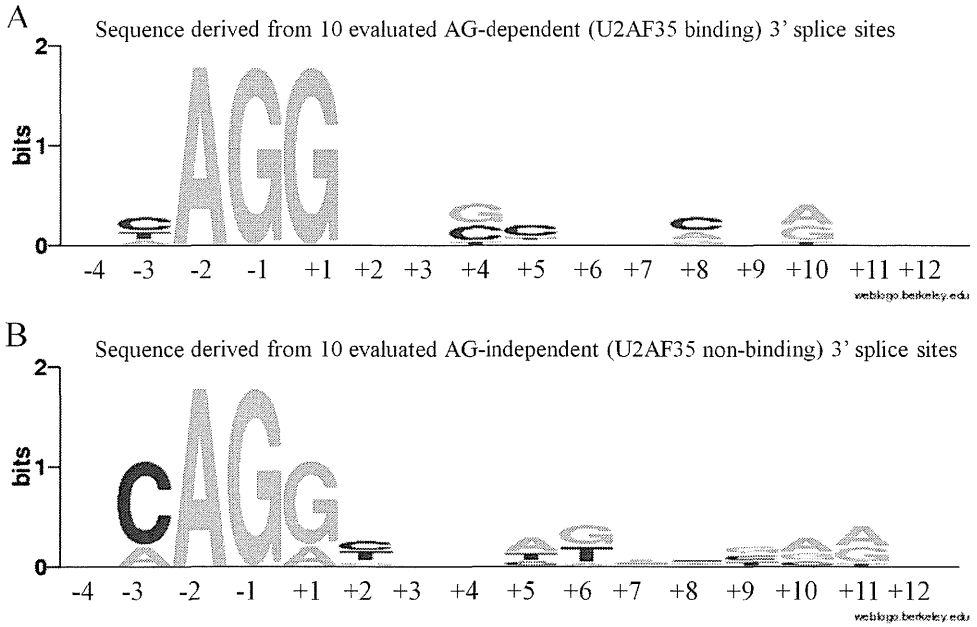

Figure 2: Sequence logos at the 3' splice sites. **A.** Ten mutations in Table 2 causing aberrant splicing. **B.** Ten mutations in Table 2 immune to aberrant splicing.

3.1.3 Exonic splicing enhancers (ESE) / Exonic splicing silencers (ESS)

It has been predicted that 16-20% of missense mutations disrupts ESEs and change the splicing pattern of the gene (Gorlov *et al.*, 2003). Comparison of effects of mutations in HGMD and neutral SNPs in dbSNP on ESE/ESS hexamers and subsequent validation of an example of *de novo* generated ESSs revealed that 7,154 out of 27,681 missense and nonsense mutations (26%) are likely to cause exon skipping (Sterne-Weiler *et al.*, 2011). Indeed, we reported that E154X and EF157V in the *CHRNE* gene (Ohno *et al.*, 2003) and E415G in the *COLQ* gene (Kimbell *et al.*, 2004) in congenital myasthenic syndromes were not nonsense or missense mutations, but were splicing mutations. Although the predicted ratios of 16-26% may be too high, many ESE/ESS-disrupting mutations are likely to be underestimated.

Although ESEs/ESSs are poorly conserved and difficult to predict, several motif search tools are available online: ESE finder 3.0 (Cartegni *et al.*, 2003), ESRsearch (Goren *et al.*, 2006), FAS-ESS (Wang *et al.*, 2004), PESXs (Zhang&Chasin, 2004) (Zhang *et al.*, 2005), RESCUE-ESE (Fairbrother *et al.*, 2002), Human Splicing Finder (Desmet *et al.*, 2009), SpliceAid (Piva *et al.*, 2009), and SpliceAid2 (Piva *et al.*, 2009). Two additional prediction algorithms employ different parameters to predict auxiliary splicing elements including ESE/ESS/ISE/ISS. CRYP-SKIP is based on a dataset of 250 skipped exons and 204 activated cryptic splice sites due to disease-causing mutations (Divina *et al.*, 2009). Spliceman is based on positional distributions of hexamers that comprise auxiliary splicing elements. Spliceman calculates the "L1 distance", which is a measure how much a mutation changes the position of a cluster of hexamers (Lim *et al.*, 2011). As these predictive algorithms tend to show false positives, *in vivo* and/or *in vitro* splicing analyses are essential to prove the splicing effect of a mutation. But it must be kept in mind that these web sites are easily discontinued and difficult to maintain due to accelerating development of new tools.

4 NAS and NASRE

4.1 Nonsense-associated altered splicing (NAS) and NMD-associated skipping of a remote exon (NASRE)

Originally found in the fibrillin gene (Dietz *et al.*, 1993; Dietz&Kendzior, 1994), a premature terminating codon (PTC) sometimes leads to aberrant splicing, which is known as nonsense-associated altered splicing (NAS) (Hentze&Kulozik, 1999). Involvement of NMD as a cause of NAS has been suggested (Mendell *et al.*, 2002; Wang *et al.*, 2002). Disruption of an ESE is also indicated as a cause of NAS (Caputi *et al.*, 2002; Liu *et al.*, 2001). Another mechanism, suppression of splicing (SOS), in which neither NMD nor ESE is involved, is also proposed (Wachtel *et al.*, 2004). As PTC itself has no effect on efficiency of removal of an adjacent intron (Lytle&Steitz, 2004), NAS is likely to be mediated by disruption of an ESE. In addition to an effect of ESEs on splicing, disruption of ESEs also stabilize pre-mRNA by unknown mechanisms (Imam *et al.*, 2010; Muhlemann *et al.*, 2001) .

A mutation can also induce skipping of a remote exon on which the mutation is not located. In congenital myasthenia syndrome, we found that a 7-bp deletion in *CHRNE* exon 7 leads to skipping of the preceding exon 6 of 101 bp, and we named it NMD-associated skipping of a remote exon (NASRE). Exon 6 has weak splicing signals and is skipped even in normal conditions. The exon 6-skipped product, however, is completely degraded by NMD due to a PTC generated by a frameshift. When exon 7 has a 7-bp deletion, the open reading frame is resumed and the exon 6-skipped product becomes immune to NMD (Ohno *et al.*, 2003). We reported other examples of NASRE, but NASRE is likely to be underestimated because remote exons are rarely scrutinized in the analysis of human diseases.

Conclusions

We have summarized canonical and auxiliary splicing *cis*-elements in physiological and pathological conditions. We hope to emphasize that splicing *cis*-elements can be located anywhere on the exon and intron, and aberrant splicing may be observed in any disease in any tissue. As correction of aberrant splicing by antisense oligonucleotides and small molecules are intensively sought for by many investigators, the identification of splicing-disrupting mutations is essential for understanding disease mechanisms and also for ameliorating pathomechanisms.

References

Beckmann, J. S.&Trifonov, E. N. (1991). "Splice junctions follow a 205-base ladder." Proceedings of the National Academy of Sciences of the United States of America 88,2380-2383.

Berget, S. M. (1995). "Exon recognition in vertebrate splicing." The Journal of biological chemistry 270,2411-2414.

Bian, Y., et al. (2009). "Tannic acid facilitates expression of the polypyrimidine tract binding protein and alleviates deleterious inclusion of CHRNA1 exon P3A due to an hnRNP H-disrupting mutation in congenital myasthenic syndrome." Human molecular genetics 18,1229-1237.

Bianchi, P., et al. (1997). "A variant of the EPB3 gene of the anti-Lepore type in hereditary spherocytosis." British journal of haematology 98,283-288.